Eur. Phys. J. B **19**, 207–213 (2001)

THE EUROPEAN PHYSICAL JOURNAL B

EDP Sciences
© Società Italiana di Fisica
Springer-Verlag 2001

Local structure of Co and Ni in decagonal AlNiCo investigated by polarized EXAFS

O. Zaharko[1,a], C. Meneghini[2], A. Cervellino[3], and E. Fischer[4]

[1] ETH Zurich & PSI Villigen, Laboratory for Neutron Scattering, Switzerland
[2] Istituto Nazionale di Fisica della Materia (INFM), c/o ESRF GILDA CRG BP 220 38043 Grenoble, France
[3] ETH Zurich, Laboratory of Crystallography, Switzerland
[4] ETH Zurich, Institute of Applied Physics, Switzerland

Received 26 July 2000 and Received in final form 20 October 2000

Abstract. The local structure of cobalt and nickel in single crystals of decagonal quasicrystals with composition $Al_{71.5}Ni_{15.5}Co_{13}$ and $Al_{75}Ni_{14.5}Co_{10.5}$ have been studied by polarized EXAFS. Significant differences between the Ni and Co local environments have been detected. The effective absence of the 4 Å periodicity along the decagonal axis in these QCs is confirmed and indications about its reasons are presented.

PACS. 61.44.Br Quasicrystals – 61.10.Ht X-ray absorption spectroscopy: EXAFS, NEXAFS, XANES, etc.

1 Introduction

The structure of quasicrystals (QCs), crystals having quasiperiodic long-range order and non-crystallographic symmetry, is a subject of considerable interest [1,2]. Several X-Ray Diffraction (XRD) studies have been addressed to the problem of QC structure determination. A first simplified model [3] of the basic decagonal (*d*-) phase of $Al_{70}Ni_{30-x}Co_x$ ($x = 7-20$) has been derived by the maximum-entropy method. The model structure (space group $P10_5/mmc$) is periodic along the **c** direction ($c = 4.0855$ Å) and consists of two flat equispaced quasiperiodic layers related by inversion. This model gives a fair illustration of the major structural features but some aspects deserve further investigation. The Edagawa superstructure is closely related [4–7] to the basic decagonal phase. However, the superstructure and the transition between the two phases [8] are still poorly known.

The most effective structure parametrization of QCs is given within the *n*-dimensional embedding technique. In the case of decagonal phases, the addition of two auxiliary dimensions (constituting the *perpendicular* or *internal* space) to the three physical coordinates consents to recover periodicity and to incorporate long-range order. The structural information is contained in the geometry of the atomic surfaces and their partition in sub-polygons. Each sub-polygon corresponds to a different coordination polyhedron and therefore different chemistry, occupation, static and dynamic displacements of the atomic sites; their areas correspond to frequencies of corresponding environments [9,10]. Unfortunately the available resolution in perpendicular space even using synchrotron radiation is largely insufficient to parametrize *ab initio* the atomic surfaces, so one has first to build an approximate model based on physical constraints (density, composition, interatomic distances) and every other available information [10] and successively refine it with the XRD data. The presence of micro-twinning and the doubling of the **c** period indicated by diffuse scattering [11] makes this task even more difficult in *d*-AlNiCo phases. Furthermore Ni and Co are not easily distinguishable by X-rays, while their different role is crucial in stabilizing the different QC phases.

Extended X-ray Absorption Fine Structure (EXAFS) is a suitable complementary technique to XRD thanks to its local sensitivity and chemical selectivity [12–16]. The complexity of QC structure and the poor knowledge *a priori* of their local structure may tangle the interpretation of the EXAFS signal and require an accurate data analysis. Up to now EXAFS was rarely applied to QCs, only one EXAFS study is reported for the *d*-AlNiCo system [17]. This work, however, was qualitative and further studies are desirable.

The aim of the present study is to probe the local atomic structure around Co and Ni in single crystals of *d*-AlNiCo employing the EXAFS technique and advanced data analysis. The polarization dependence of EXAFS signal has been exploited to study anisotropy of the QC along and normal to the 10-fold **c** axis. In this work we address the two main questions which are still a challenge for QC crystallographers, namely:

1. What is the difference between the local atomic environments of nickel and cobalt atoms?
2. Which kind of perturbation is responsible for the doubling of the **c** period?

[a] e-mail: Oksana.Zaharko@psi.ch

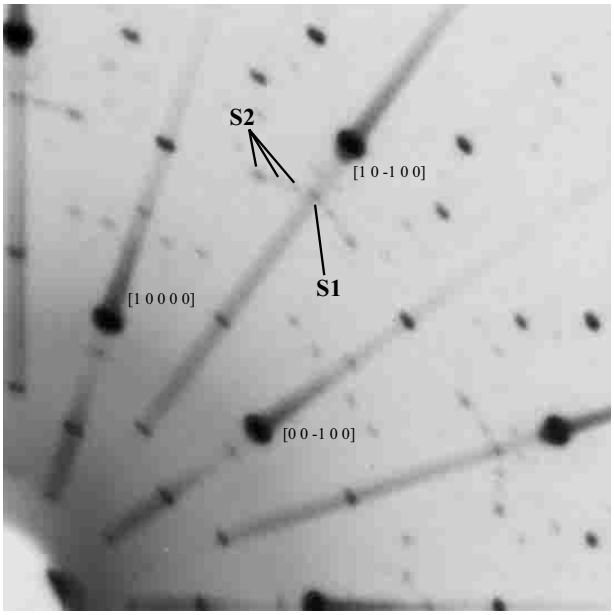

Fig. 1. Precession photograph of the $hk0$-layer of the representative sample III. Some main reflections are indexed for reference (setting of Ref. [3] for the basic decagonal phase). Both the S1 and S2 satellite classes are clearly visible (*cf.* Ref. [6]).

2 Experimental and data analysis

Two large single crystals having nominal compositions $Al_{71.5}Ni_{15.5}Co_{13}$ and $Al_{75}Ni_{14.5}Co_{10.5}$ were used for this study. The first crystal (sample I) was kindly loaned by B. Grushko (Forschungszentrum Jülich). The second crystal was grown by Bridgmen method at ETH Zurich, Institute of Applied Physics, annealed at 1050 °C for 24 hours for homogenization and cut into two parts (samples II and III). All samples have been characterized by the Laue and precession methods (Mo K_α radiation). They have been oriented and faces parallel and normal to the 10-fold **c** axis were cut. The samples show decagonal diffraction patterns (Fig. 1) and have good crystal quality. The clear evidence of both S1 and S2 satellites indicates ordering into the decagonal Edagawa superstructure.

The X-ray Absorption Spectroscopy (XAS) spectra have been collected at the BM29 beamline [18] at the European Synchrotron Radiation Facility (ESRF) in Grenoble (France). Beam energies were defined by a double crystal Si [111] monochromator. XAS spectra at the Co (7709 eV) and Ni (8833 eV) K edges were collected in total electron yield geometry and the incident photon flux for data normalization was measured using an Ar-filled ionization chamber. Samples were mounted in a closed-cycle He refrigerator and cooled down to 70 K to reduce the effects of thermal motion on the structure. The EXAFS structural signal $\chi(k)$ is defined as the relative oscillations of the total absorption coefficient $\mu(k)$ with respect to the absorption coefficient of the isolated atom $\mu_0(k)$ [19], where k is the modulus of photoelectron wave vector. In the EXAFS region, that starts some tenth of eV above the absorption edge, the structural information contained in the $\chi(k)$ may be expressed by the formula [13]:

$$\chi(k) = S_0^2 \sum_i \frac{N_i^*}{kR_i^2} A_i(k) \mathrm{e}^{-2R_i/\lambda(k)} \mathrm{e}^{-2k^2\sigma_i^2} \times \sin(2kR_i + \delta_{0i}(k)) \quad (1)$$

valid in single scattering approximation for N_i^* neighbours distributed on the ith Gaussian shell at the average distance R_i with the variance σ_i^2 (Debye-Waller factor). $A_i(k)$ and $\delta_{0i}(k)$ are respectively the backscattering amplitude and phase shift function for the absorber-neighbour pair. The factor $\mathrm{e}^{-2R_i/\lambda(k)}$ takes into account the signal attenuation due to the photoelectron mean free path and core-hole life time, while S_0^2 accounts for losses due to many-body effects. In anisotropic systems N_i^* is the *polarization-dependent effective coordination number*:

$$N_i^* = 3 \sum_{j=1}^{N_i} \cos^2(\theta_{ij}) \quad (2)$$

where $\theta_{ij} = \widehat{\boldsymbol{\epsilon}} \angle \mathbf{R}_{ij}$ is the angle between the electric field vector $\mathbf{E}$ of the incoming beam and the radius connecting the absorber to the jth neighbour atom in the ith coordination shell. The XAS spectra of the three AlNiCo samples were collected with the 10-fold **c** axis oriented along ($\mathbf{E} \parallel \mathbf{c}$) and normal ($\mathbf{E} \perp \mathbf{c}$) to the electric field vector $\mathbf{E}$. As follows from equation (2), in fact, only the neighbours with $z \neq 0$ contribute to the EXAFS signal measured with $\mathbf{E} \parallel \mathbf{c}$. Similarly, only those neighbours which have nonzero components in the (xy) plane contribute to the total EXAFS signal for the $\mathbf{E} \perp \mathbf{c}$ orientation.

EXAFS data analysis was performed using the theory developed in references [14,19] and implemented in the GNXAS package [15]. Within this approach the contributions to the $\chi(k)$ of the atomic environment around the absorber are decomposed in terms of irreducible n-body contributions $\gamma^{(n)}$. This allows to relate directly the EXAFS spectra with the n-body correlation functions, g_n, of the system under investigation. Moreover, the fitting procedure is performed directly on the raw data without passing through a Fourier filtering procedure, this allows a rigorous error analysis on the fitting parameters and an accurate statistical evaluation of the best fit quality [15]. For these reasons we estimate the GNXAS approach particularly suitable and reliable for the analysis of EXAFS data of disordered materials.

The polarized Co and Ni EXAFS signals, $\chi(k)$, for all measured samples are shown in Figure 2. Their Fourier transforms, representing the structural features around the absorber, are reported in Figure 3 for the representative sample I. Even from visual inspection it is evident that the local structure of Co and Ni is dominated by the nearest-neighbour correlations (first shell). This holds for all studied samples. The weak and broad next-neighbour contributions suggest large variations and/or distortions of the local environment at distant shells of both Co and Ni. The differences between $\mathbf{E} \parallel \mathbf{c}$ and $\mathbf{E} \perp \mathbf{c}$ data are small, indicative for quite isotropic local environment of transition metal atoms. The EXAFS signals of Co

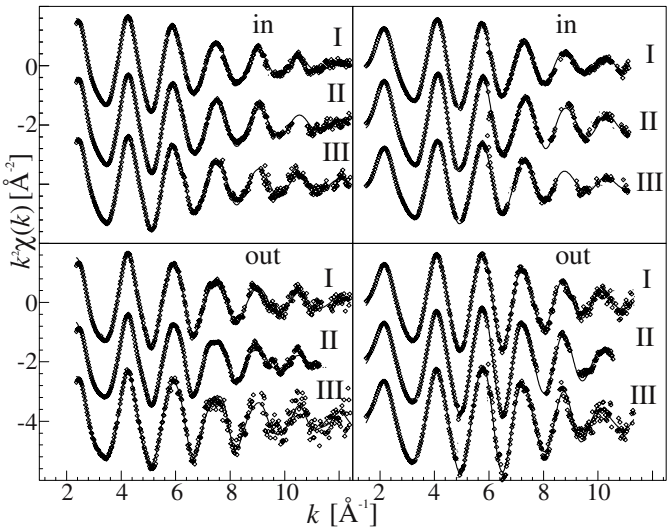

Fig. 2. Measured polarized Co (left) and Ni (right) K edge EXAFS signals for the three studied samples (I–III) in the $\mathbf{E} \parallel \mathbf{c}$ (out) and $\mathbf{E} \perp \mathbf{c}$ (in) geometries. The total model EXAFS signal is given by solid lines.

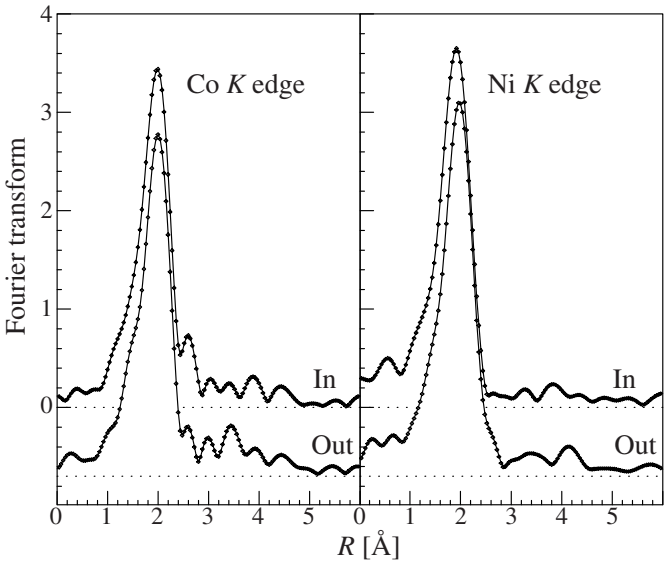

Fig. 3. The Fourier transforms of the signals reported in Figure 2 at the Co (left) and Ni (right) K edges in the $\mathbf{E} \parallel \mathbf{c}$ (out) and $\mathbf{E} \perp \mathbf{c}$ (in) geometries.

and Ni seem rather similar, but careful expection of Figure 2 allows to distinguish a broadening of the Co $\mathbf{E} \perp \mathbf{c}$ EXAFS oscillation in the region of 6–9 Å^{-1} compared to Ni. To highlight the differences between Co/Ni and in-plane/out-of-plane EXAFS data, Figure 4 presents the backscattering amplitude $A_i(k)$ and phase shift $\delta_{0i}(k)$ calculated from the back Fourier transforms of the nearest-neighbours peak. A significant phase shift between the Co and Ni $\mathbf{E} \parallel \mathbf{c}$ EXAFS data (bottom panel) is observed. This is mainly due to the different photoabsorber involved. The in-plane amplitude functions (top panel), however, are similar for the both edges. For the Ni K edge a large difference between the in-plane and out-of-plane amplitudes appears around 6 Å^{-1}. This implies larger contributions of transition metal neighbours along **c**. In fact, $A_{\mathrm{Ni}}(k)$ and $A_{\mathrm{Co}}(k)$ have an evident maximum between 6 and 7 Å^{-1}, respectively, while $A_{\mathrm{Al}}(k)$ decreases monotonously [20].

Modelling the EXAFS signal the following peculiarities must be taken into account:

1. It is not possible to distinguish cobalt and nickel as the backscattering atoms, because the EXAFS signals generated by the two-body contributions $\gamma_{\mathrm{T,Co}}$ and $\gamma_{\mathrm{T,Ni}}$ (T = Co or Ni) are very similar. However, cross-checking the different environments partially overcomes this problem.
2. It is easy to distinguish the Al- or T-neighbours, if one considers the isolated EXAFS signals. This is due to a large difference in their amplitude and phase functions: the $\gamma_{\mathrm{T,Al}}$ amplitude decreases with k, while the $\gamma_{\mathrm{T,T}}$ amplitude shows a maximum around 5 Å^{-1}. However, in a mixed EXAFS signal the large phase shift for the Al- and T-neighbours produces an anti-phase effect leading to a large uncertainty in the coordination numbers. In some cases it is not possible to distinguish contribution of a one-component shell and exceeding part of a bimodal shell.
3. The sensitivity to next-neighbour shells decreases with the distance due to the contributions of the mean-free-path term and the R^{-2} factor in equation (1), and due to the absence of the periodic long-range order within the quasiperiodic layers. This strongly reduces the accuracy on the structural parameters of the next-neighbour shells.

We used the following refinement procedure. Firstly, the EXAFS signal was modelled including only the dominant contributions of the first-neighbour shell and refined simultaneously with the polynomial spline, which modelled the atomic background $\mu_0(k)$ and threshold energy E_0. Then the $\mu_0(k)$ and E_0 refinement was stopped and the contributions of the next-neighbour shells were added one by one. If the fitted signal significantly improved the residual (χ^2-test), the shell was included into the EXAFS model and a next shell was checked.

No significant improvement was achieved including the next-neighbour shells farther than 5 Å. The two-body contributions dominate the EXAFS signals of the studied samples and the multiple scattering effects can be neglected in the modelling of our data. Figure 5 presents the best fit of the Co and Ni $\mathbf{E} \perp \mathbf{c}$ EXAFS data for the sample I together with the partial contributions and final residuals. All studied samples possess similar structural features, though the qualitative parameters vary slightly (see Tab. 1).

The Co K edge EXAFS signals are dominated by a one-component first shell composed of Al atoms at a distance 2.42 Å. The effective coordination numbers are similar for the $\mathbf{E} \parallel \mathbf{c}$ and $\mathbf{E} \perp \mathbf{c}$ orientations being in the range of 6.3 to 7.

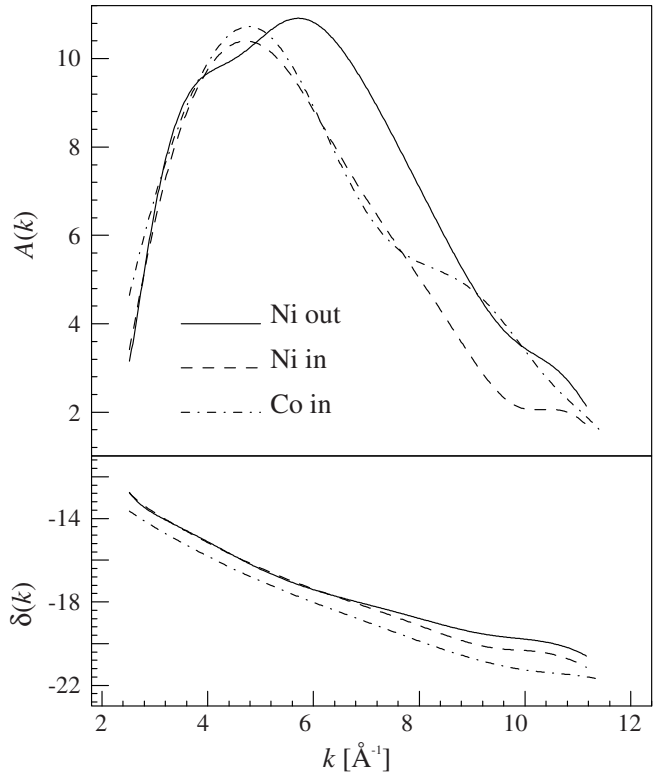

Fig. 4. The backscattering amplitude A_i(k) (top) and phase shift δ_{0i} (bottom) calculated from the back Fourier transform of the nearest neighbours peak of the Ni and Co EXAFS data according to the standard EXAFS analysis (*cf.* Ref. [13]).

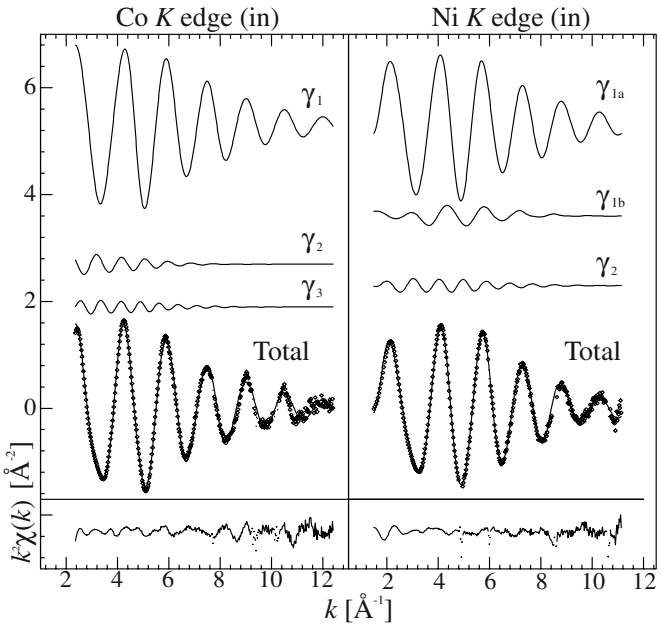

Fig. 5. The experimental signal reported in Figure 2, total model EXAFS signal and their difference for Co (left) and Ni (right) for the $\mathbf{E} \perp \mathbf{c}$ geometry.

The nearest-neighbour shell around Ni presents a bimodal distribution with the Al atoms ($N^* = 7$ to 8) at around 2.46 Å and the T atoms ($N^* \approx 3$) at 2.65–2.67 Å. This shell accounts for the differences in the amplitude function $A_i(k)$ shown in Figure 4. The Debye-Waller factor for the Ni-T contribution for $\mathbf{E} \perp \mathbf{c}$ is three times larger compared to $\mathbf{E} \parallel \mathbf{c}$. This large disorder reduces the weight of corresponding contributions and makes the amplitudes $A_i(k)$ for the in-plane Ni and Co environment similar. The distance 2.65–2.67 Å is known from the structure model to be characteristic of interstitial (inter-layer) atoms. These sites are often referred to as 'icosahedral caps' because they are part of distorted Al-T icosahedra. The Co data do not show a Co-T shell at this distance, therefore the Ni-T shell must be composed of Ni-Ni pairs. The Ni-Al contributions are almost the same for the $\mathbf{E} \parallel \mathbf{c}$ and $\mathbf{E} \perp \mathbf{c}$ orientations, except for the sample III, where the Ni-Al effective in-plane coordination number N^*_{in} is clearly reduced with respect to the out-of-plane value N^*_{out}. The in-plane Ni-Ni contributions display the larger σ^2 values in all samples suggesting a more ordered arrangement along the **c** axis compared to that in the decagonal plane.

The difference between the $\mathbf{E} \parallel \mathbf{c}$ and $\mathbf{E} \perp \mathbf{c}$ orientations becomes more significant in the next-neighbour distributions. The Co data analysis reveals two next-neighbour shells at about 3.9 Å and 4.8 Å dominated by Co-Al contributions. The effective coordination numbers and Debye-Waller factors of the second shell increase 2 to 3 times for the $\mathbf{E} \parallel \mathbf{c}$ orientation comparing to the corresponding values for $\mathbf{E} \perp \mathbf{c}$. Similar conclusions can be deduced from the third coordination shell of cobalt. This general tendency reflects the peculiarity of *d*-QCs, namely, the long-range periodic order along **c** and the long-range quasiperiodic order normal to **c**.

The Ni next-neighbour shells also show anisotropy effects. But in addition to the feature mentioned for Co, qualitative differences are present. The EXAFS signal in the $\mathbf{E} \parallel \mathbf{c}$ orientation is dominated by the Ni-T shell at around 3.6 Å, while for the $\mathbf{E} \perp \mathbf{c}$ orientation the Ni atoms are surrounded by the Al-neighbours at about 4 Å. The out-of-plane Ni data also display a distant shell around 4.9 Å as for Co but with larger disorder. This shell cannot be detected in the decagonal plane.

In order to check the reliability of the differences in the Ni and Co local environment, we tried to exchange the models. More precisely, we fitted the Co data with the bimodal nearest-neighbour shell formerly determined for Ni and similarly the Ni data with the one-component first shell of Co. The fit results significantly worse in both cases, as shown in Figure 6 for the Ni $\mathbf{E} \parallel \mathbf{c}$ EXAFS signal.

3 Discussion

The performed polarized EXAFS study revealed important details of the local environment of the transition metal atoms in *d*-AlNiCo.

Firstly, we observe different local environments for Co and Ni, in contrast to the findings of reference [17]. Nickel has a bimodal nearest-neighbour surrounding with

Table 1. EXAFS results for samples I, II and III. $N^*_{\rm out}$ and $N^*_{\rm in}$ are the effective coordination numbers for the $\mathbf{E} \parallel \mathbf{c}$ and $\mathbf{E} \perp \mathbf{c}$ geometries. Statistical errors on the structural parameters were estimated according to reference [16].

	Co					
shell	R, Å	$N^*_{\rm out}$	σ^2, Å^2	R, Å	$N^*_{\rm in}$	σ^2, Å^2
			sample I			
1	2.42(1)	6.9(3) Al	0.0057(3)	2.43(1)	7.1(3) Al	0.0063(3)
2	3.9(2)	2.4(4) Al	0.010(2)	4.0(2)	5.0(4) Al	0.030(2)
3	4.8(3)	3.3(7) Al	0.009(2)	4.8(3)	4.6(7) Al	0.022(2)
			sample II			
1	2.42(1)	6.6(3) Al	0.0049(3)	2.42(1)	7.0(3) Al	0.0056(3)
2	3.9(2)	2.5(4) Al	0.0070(2)	4.0(2)	5.2(4) Al	0.033(1)
3	4.8(3)	3.2(7) Al	0.0056(3)	4.3(3)	4.8(8) Al	0.018(2)
			sample III			
1	2.42(1)	6.3(3) Al	0.0040(3)	2.42(1)	6.8(3) Al	0.0058(3)
2	3.9(2)	2.5(4) Al	0.0061(2)	4.0(2)	5.7(4) Al	0.039(1)
3	4.8(3)	2.9(7) Al	0.0024(3)	4.8(3)	3.3(8) Al	0.012(2)

	Ni					
shell	R, Å	$N^*_{\rm out}$	σ^2, Å^2	R, Å	$N^*_{\rm in}$	σ^2, Å^2
			sample I			
1	2.47(1)	7.6(6) Al	0.0067(4)	2.46(1)	8.3(6) Al	0.0080(4)
	2.65(1)	2.2(6) T	0.0083(4)	2.67(1)	3.6(6) T	0.0280(4)
2	3.6(2)	1.5(4) T	0.0089(2)	4.0(2)	2.5(4) Al	0.012(1)
3	4.9(3)	4.4(7) Al	0.025(3)			
			sample II			
1	2.46(1)	7.8(6) Al	0.0058(4)	2.45(1)	8.3(6) Al	0.0071(4)
	2.68(1)	2.7(6) T	0.0090(4)	2.65(1)	3.4(6) T	0.0282(4)
2	3.7(2)	1.4(4) T	0.0089(3)	4.0(2)	3.1(4) Al	0.013(1)
3	4.9(3)	5.0(8) Al	0.029(4)			
			sample III			
1	2.46(1)	8.1(6) Al	0.0066(4)	2.46(1)	6.9(6) Al	0.0074(4)
	2.63(1)	2.4(6) T	0.0068(4)	2.67(1)	2.4(6) T	0.0223(4)
2	3.6(2)	1.9(4) T	0.0070(3)	4.0(2)	2.8(4) Al	0.015(1)
3	4.9(3)	5.0(8) Al	0.030(4)			

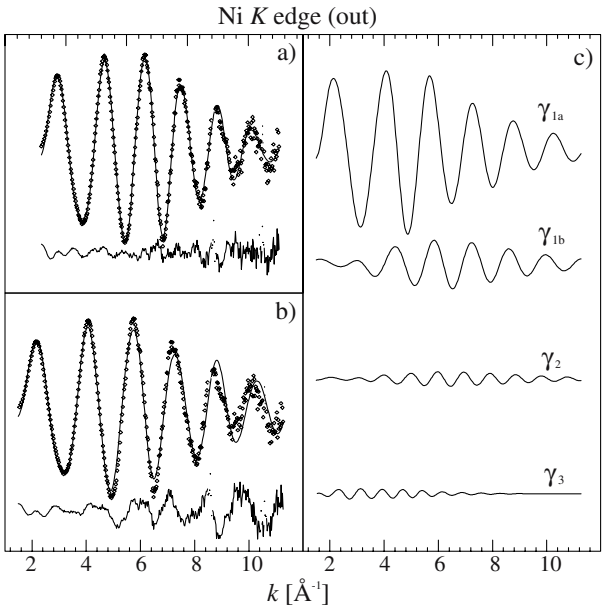

Fig. 6. The experimental and calculated Ni $\mathbf{E} \parallel \mathbf{c}$ EXAFS signals. The model with the bimodal first shell (a) fits the observations significantly better than the model with the one-component first shell (b). The individual contributions of the next-neighbour shells of the final model (a) are presented in (c).

Al atoms at the distance of about 2.46 Å and T (Ni) about 2.67 Å. For cobalt such bimodal distribution cannot be excluded, but it is less evident: the model with only Al atoms in the first shell at around 2.42 Å agrees better with the experiment. These conclusions are in a good agreement with the assumption of reference [3] that Co atoms are surrounded only by Al. It is worth noting that the Co-Al distances (2.42 Å) are systematically lower than the Ni-Al distances (2.46 Å) as it was proposed in reference [3] for chemical reasons.

Secondly, our data depict a higher degree of order along the **c** axis compared to the decagonal plane due to the periodic and quasiperiodic long-range order, respectively.

Thirdly, the absence of the T-T correlations around 4 Å in the $\mathbf{E} \parallel \mathbf{c}$ measurements confirms the effective absence of the 4 Å periodicity along the decagonal axis in these QCs and gives some indications about its reasons. In fact, the sites at 4 Å along **c** are rather depopulated, while periodicity would imply their full occupation. Let us conservatively assume that the whole $\mathbf{E} \parallel \mathbf{c}$ EXAFS signal at ≈4 Å is generated by atoms along **c**. Then the Co atoms are intercalated with Al atoms along the **c** axis at a 3.93 Å distance with the coordination number $N = 0.78-0.84$. As the expected value would be 2, this means that the intercalating Al sites are often vacant. For the Ni atoms the situation is different as no neighbours at 4 Å distance along **c** are found. On one side, there is a Ni-Ni distance, shortened to about 3.65 Å with the coordination number of these sites $N = 0.46-0.64$. On the other side, there is a Ni-Al distance expanded to about 4.8 Å with $N = 1.46-1.68$.

These facts are strongly incompatible with the average **c**-periodicity of 4 Å. However, they are compatible with the effective periodicity of 8 Å, which is revealed by interlayer diffuse scattering, but whose origin is not yet well understood. The relevant coherence length along the **c** direction is high ($\approx 10^4$ Å), while it is very low in the quasiperiodic plane ($< 10^2$ Å). Hence *d*-AlNiCo consists of well ordered columns parallel to **c**, having frequent

misalignments (*cf.* Ref. [11]) and no stacking disorder is present. In scope of these findings the present results acquire more relevance and can be useful for directing further research. In particular, we can exclude that the 8 Å superordering is only due to ordering of the Al sites.

The local structure obtained by EXAFS has common features with the average XRD model, though there is also some divergence. The model that we use for comparison has been adapted from the 5-D structure model that has been used to describe the basic d-$Al_{71}Ni_{22}Co_7$ phase and to refine its structure with a synchrotron high-resolution XRD data set and will be published elsewhere [21,22]. It has been simplified to allow for slight structural differences in the different d-phase (Edagawa superstructure) of our samples. Especially the occupational correlation of neighboring partly occupied sites has been neglected, keeping a consistent number of degrees of freedom. According to this model, the atoms of transition metal may be classified as belonging to three different clusters, A, B and C, corresponding also to distinct subregions of the atomic surfaces. The calculations of the EXAFS effective coordination numbers have been performed according to equation (2). In detail, from the 5-D structure model all the atomic sites in a 40 nm×40 nm×0.8 nm box have been derived. Successively, the uncorrelated-occupancy-weighted effective coordination numbers have been calculated for *every* T atom in the structure and for every neighboring shell, the averages (general and by cluster) being performed at the end. These results are presented for comparison in Table 2, listing the EXAFS parameters of these clusters, namely, the distance R from the central atom and the effective coordination number N^* for the $\mathbf{E} \parallel \mathbf{c}$ and $\mathbf{E} \perp \mathbf{c}$ experimental geometries. In addition we list the distribution of the T atoms (Δ) in the clusters and what part of the total T-content this represents (δ). There is no direct information about the Co/Ni distribution from XRD. However, from comparison with other Al-rich phases with Ni and/or Co the distribution of Co between the A, B, C clusters may be inferred [22]. It is plausible that nickel occupies cluster C, cobalt cluster A and both can be found in cluster B, depending on the QC composition.

The EXAFS and XRD models agree that the first shell is composed of majority Al and minority T atoms. However, the XRD model implies the same distance for both Al and T atoms and this distance is slightly larger with respect to the EXAFS first shell. Besides, the XRD model allows a few atoms to have a 2.96 Å distance (clusters A and B) for the $\mathbf{E} \perp \mathbf{c}$ geometry but they are not detected by EXAFS. This distance is known [6] to be present and very frequent in the structure, being the typical nearest-neighbor Al-Al distance. The EXAFS results clarify that this distance is not significantly present for T-Al or T-T pairs.

Both models show large anisotropy effects on the next-neighbour shells. The XRD model indicates the presence of T atoms in the second shell for the $\mathbf{E} \parallel \mathbf{c}$ geometry ($N^* = 6$ for the cluster C), but according to EXAFS there are no T atoms at 4 Å for cobalt and they are shifted to 3.6–3.7 Å for nickel. The XRD model includes a number of atoms at a 4.56 Å distance from the cluster center, but their contribution is not significant to the EXAFS signal. The XRD model of the third shell implies that there is almost equal amount of the Al and T atoms for the $\mathbf{E} \perp \mathbf{c}$ geometry, while the Al atoms dominate for $\mathbf{E} \parallel \mathbf{c}$. This statement is in agreement with the Ni edge EXAFS model, but contradicts the Co edge results.

The EXAFS results, however, confirm some controversial features of the XRD model. There are positive indications of chemical Al-T disorder (at least for the average 4 Å structure) and the presence of a significant fraction of partially occupied sites, which was inferred from the bond-length analysis [10,11] and is strongly plausible for the basic d-phase [21,22].

Table 2. XRD model of the basic decagonal structure $Al_{71}Ni_{22}Co_7$ [21]. The distance R between the central cluster atom and the neighbours and effective coordination numbers N^* are listed. Δ is the distribution of the T atoms in the cluster center (the rest is aluminum), δ shows which part of the total T-content this is.

Cluster		A		B		C	
shell	R, Å	N^*_{out}	N^*_{in}	N^*_{out}	N^*_{in}	N^*_{out}	N^*_{in}
1 Al	2.52	8.83	6.02	7.59	5.10	6.74	9.68
T		2.59	0.75	3.80	1.10	2.07	1.32
Al	2.96	-	1.85	-	0.99	-	-
T		-	1.22	-	2.30	-	-
2 Al	3.90	3.06	2.02	4.41	6.41	-	-
T		2.04	-	1.5	0.56	6	-
Al	4.56	5.32	10.6	3.8	7.56	6.60	13.14
T		2.18	4.34	1.5	2.99	4.00	7.96
3 Al	4.8-5.05	14.9	5.04	10.97	3.17	15.69	5.70
T		3.19	5.06	6.04	5.54	-	4.52
Δ, %		40		36		100	
δ, %		6.7		3.7		18.53	

The authors are grateful to Dr. B. Grushko for providing the $Al_{71.5}Ni_{15.5}Co_{13}$ single crystal, to the BM29 beamline group at ESRF for excellent support, to Ms. M. Krichel for taking the precession photographs, and to Prof. W. Steurer for stimulating discussions. The research on the model structure (A.C.) was funded by the Swiss National Science Foundation, contract No. 20-53630.98.

References

1. C. Janot, *Quasicrystals* (Clarendon Press, Oxford 1994), p. 409.
2. W. Steurer, T. Haibach, in *Physical properties of Quasicrystals*, edited by Z. Stadnik (Springer, Heidelberg-New York, 1999), pp. 51–90.

3. W. Steurer, T. Haibach, B. Zhang, S. Kek, R. Lück, Acta Crystallogr. B **49**, 661 (1993).
4. K. Edagawa, M. Ichihara, K. Suzuki, S. Takeuchi, Phil. Mag. Lett. **60**, 16 (1992).
5. M.A. Estermann, T. Haibach, W. Steurer, Phil. Mag. Lett. **70**, 379 (1994).
6. T. Haibach, A. Cervellino, M.A. Estermann, W. Steurer, Phil. Mag. A **79**, 933 (1999).
7. A. Yamomoto, S. Weber, Phys. Rev. Lett. **79**, 861 (1997).
8. T. Haibach, M.A. Estermann, A. Cervellino, W. Steurer, J. Mater. Sci. Eng. A **294-296**, 17 (2000).
9. A. Cervellino, T. Haibach, W. Steurer, J. Mater. Sci. Eng. A, **294-296**, 276 (2000).
10. T. Haibach, A. Cervellino, M.A. Estermann, W. Steurer, Z. Kristallogr. **215**, 569 (2000).
11. W. Steurer, F. Frey, Phase Transitions **67**, 319 (1998).
12. J. Stöhr, *NEXAFS Spectroscopy* (Springer, Berlin, 1992), p. 403.
13. P.A. Lee, P.H. Citrin, P. Eisenberger, B.M. Kincaid, Rev. Mod. Phys. **53**, 769 (1981).
14. A. Filipponi, A.D. Cicco, C.R. Natoli, Phys. Rev. B **52**, 15122 (1995).
15. A. Filipponi, A.D. Cicco, Phys. Rev. B **52**, 15135 (1995).
16. A. Filipponi, J. Phys. Cond. Matt. **7**, 9343 (1995).
17. S. Braun, D.C. Meyer, P. Paufler, B. Grushko, J. Alloys Comp. **287**, 12 (1999).
18. A. Filipponi, M. Borowski, D.T. Bowron, S. Ansell, A. Di Cicco, S. De Panfilis, J.-P. Itié, Rev. Sci. Inst. **71**, 2422 (2000).
19. M. Benfatto, C.R. Natoli, A. Bianconi, J. Garcia, A. Marcelli, M. Fanfoni, I. Davoli, Phys. Rev. B **34**, 5774 (1986).
20. A.G. McKale, J. Am. Chem. Soc. **110**, 3763 (1988).
21. A. Cervellino (2000, unpublished).
22. A. Cervellino, T. Haibach, W. Steurer, Ferroelectrics (in press).